



Micro-characteristics of High-Entropy Alloy Weld Formed by Friction Stir Lap Welding of 1060 Al and Al_{0.1}CoCrFeNi

H. J. Zhang^{1,2} · L. Y. Zhao¹ · X. Liu¹ · H. Zhang¹ · Y. L. Wang¹ · J. L. Song³

Received: 19 August 2020 / Accepted: 14 October 2020 / Published online: 28 October 2020
© The Indian Institute of Metals - IIM 2020

Abstract 1060 Al and Al_{0.1}CoCrFeNi are friction stir lap welded in this study. The limited flow of high-entropy alloy avoids the occurrences of hook and cold lap defects in the lap joint. Coarsening of large-size Al(Cr)-rich particles and dissolution of small-size Al(Cr)-rich particles simultaneously take place in the heat-affected zone of high-entropy alloy during the welding. The plastic deformation of high-entropy alloy induced by welding tool refines and homogenizes the microstructures in thermo-mechanically affected zone and stir zone. Friction stir lap weld of high-entropy alloy presents higher hardness than the base metal in each zone. The hardness of stir zone exhibits a maximum of 600 Hv, higher than the maximum hardness of Al_xCoCrFeNi traditionally obtained. This should be attributed to the microstructure refinement as well as the enhancement of solid-solution strengthening and the occurrence of body-centered-cubic structures due to Al content improvement.

Keywords High-entropy alloy · Aluminum · Friction stir lap welding · Micro-characteristic

1 Introduction

High-entropy alloys (HEAs) including five or more elements in equal or near-equiatomic compositions yield great flexibility in design of materials with outstanding properties and thus have been qualified as potential structural and functional materials in the fields of aviation, biomedicine, atomic power and energy [1–3]. Material processing including welding is inevitable for engineering applications, and the welding technology of HEAs is important for the engineering application of this type of material [4]. Investigations on welding of HEAs by various techniques have been conducted by previous researchers. Different welding processes such as arc welding [5, 6], laser welding [7, 8], electron beam welding [6, 9] and friction stir welding [10–13] have been utilized to weld HEAs. Different from arc, laser and electron beam welding, friction stir welding (FSW) is a solid-state joining technique, in which two facing workpieces are joined through the heat generated by friction between a rotating tool and the workpiece material. Owing to the attributes of solid-state joining, various welding defects commonly observed in fusion welding, such as porosity and crack, can be effectively avoided by FSW [14]. Hence, FSW has become an important and hotspot technology for the welding of HEAs in recent years. For instances, Shaysultanov et al. [10] studied FSW of a CoCrFeNiMn HEA. Owing to the microstructure refinement and increase in the volume fraction of M₂₃C₆ carbides, the weld showed a noticeable rise in strength; furthermore, the weld stir zone (SZ) presented an approximately 40 Hv increase in microhardness relative to the base metal (BM). Jo et al. [11] investigated the microstructures and mechanical properties of friction stir welded 2-mm-thick CrMnFeCoNi HEA. The results found a hardness improvement from 114 Hv of the BM to

✉ H. J. Zhang
zhanghuijie@neuq.edu.cn

¹ School of Resources and Materials, Northeastern University at Qinhuangdao, Qinhuangdao 066004, People's Republic of China

² School of Materials Science and Engineering, Northeastern University, Shenyang 110819, People's Republic of China

³ Tianjin Aerospace Long March Rocket Manufacturing Co., Ltd, Tianjin 300452, People's Republic of China

215 Hv of the SZ due to the grain refinement caused by FSW. Zhu et al. [12] studied the FSW of a 2-mm-thick face-centered-cubic (FCC) CoCrFeNiAl_{0.3} HEA. Similarly, refined equiaxed microstructures were also produced in the weld due to recrystallization, leading to higher hardness of the SZ than the BM. Additionally, the X-ray diffraction (XRD) results indicated that the HEA remained an FCC structure after FSW. Another of their study [13] performed the FSW of a Co₁₆Fe₂₈Ni₂₈Cr₂₈ HEA, which revealed a similar trend of hardness increase in the SZ compared to the BM.

It has been observed that the previous investigations on the FSW of HEAs were mainly related to the butt or bead welding. The FSW of lap joints, especially between the conventional metals and HEAs, have not been reported in the existing literatures until now. On the other hand, compared with the HEA preparation from the liquid state, mechanical alloying is a solid-state powder-processing technique featured by low fabrication temperature and finer alloy structures, which has successfully produced alloys suitable for high-heat turbine blades and other aerospace components [15, 16]. However, the investigations on the FSW of such type of HEAs still lack. The developments of effective joining technologies for different base materials and joint configurations are important for potential applications of HEAs. In light of this, friction stir lap welding (FSLW) between aluminum and a Al_xCoCrFeNi HEA characterized by excellent specific strength, low temperature mechanical properties and radiation resistance [1, 2] is conducted in this paper. The current work has been undertaken to understand the characteristics of the high-entropy alloy weld formed by the lap welding in terms of microstructures and mechanical properties.

2 Experimental Procedure

The BMs employed in this work were 1060-O Al and Al_{0.1}CoCrFeNi. The Al plate with Al content of 99.6 wt% had the dimensions of 2.8 mm × 60 mm × 100 mm. Ingots with composition of Al_{0.1}CoCrFeNi (at%) were prepared by powder metallurgy and had the dimensions of 2 mm × 60 mm × 100 mm. The surfaces of the welding samples were ground with grit paper to remove the oxide film and then cleaned by ethanol before welding. 1060 Al sheet was placed over Al_{0.1}CoCrFeNi alloy and had stiff contact to form a lap joint configuration, after which an FSW machine and a welding tool were utilized to perform the FSLW experiments. The tool shoulder (12 mm in diameter) having three equally spaced scrolls on the end surface was utilized in the study. The conical tool pin with the length of 2.85 mm had right-hand threads for counterclockwise rotation. During the welding, a shoulder

plunge depth of 0.2 mm and a tilting angle of 2° with respect to workpiece were applied to the welding tool, and the rotation speed and welding speed of the tool were kept at 800 rpm and 50 mm/min, respectively.

After the welding, the samples were cut perpendicular to the weld, ground on emery paper from 300 to 2500 grits and polished by diamond suspension. The microstructures were examined by a scanning electron microscopy (SEM) equipped with energy-dispersive spectroscopy (EDS). Vickers microhardness measurements were taken on the cross section of joint using 1000 g loading force for 15 s. A total of 337 indentations along 30 vertical directions were measured in order to obtain the hardness distribution map. Room-temperature tensile shear test was carried out on an electronic universal tensile testing machine (WDW-3100) at a constant testing speed of 1 mm/min. The lap shear specimens were 60 mm in length and 12 mm in width. The crystal structures of the fracture surface were identified by XRD using Cu K α radiation.

3 Results and Discussion

Figure 1 shows the macroscopic appearance of the lap joint, where the retreating side (RS) and the advancing side (AS) are marked in the figure. It is known that the hook and cold lap defects are commonly produced during FSLW, which may be alleviated and suppressed by improving tool designs or optimizing welding parameters [17, 18]. Compared with aluminum, the severe lattice distortions caused by different atom sizes tend to yield lower fluidities for HEAs, and the plastic flow of Al_{0.1}CoCrFeNi alloy is only restricted to a limited area around the tool during FSLW. Consequently, such hook and cold lap defects are not evident at the Al-HEA interface.

Figure 2a further offers an enlarged view of the Al-HEA interface. The lap weld in HEA can be divided into the SZ,

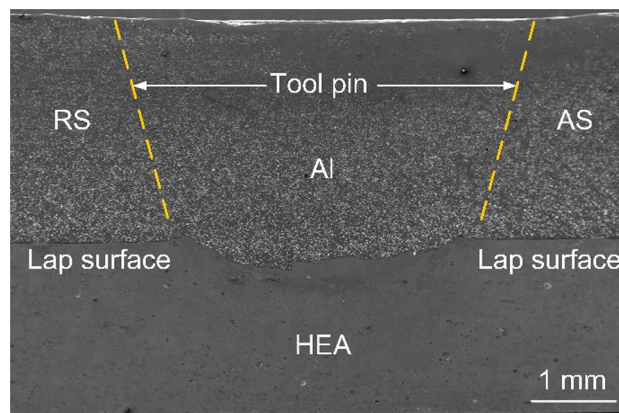


Fig. 1 Cross section of the lap joint

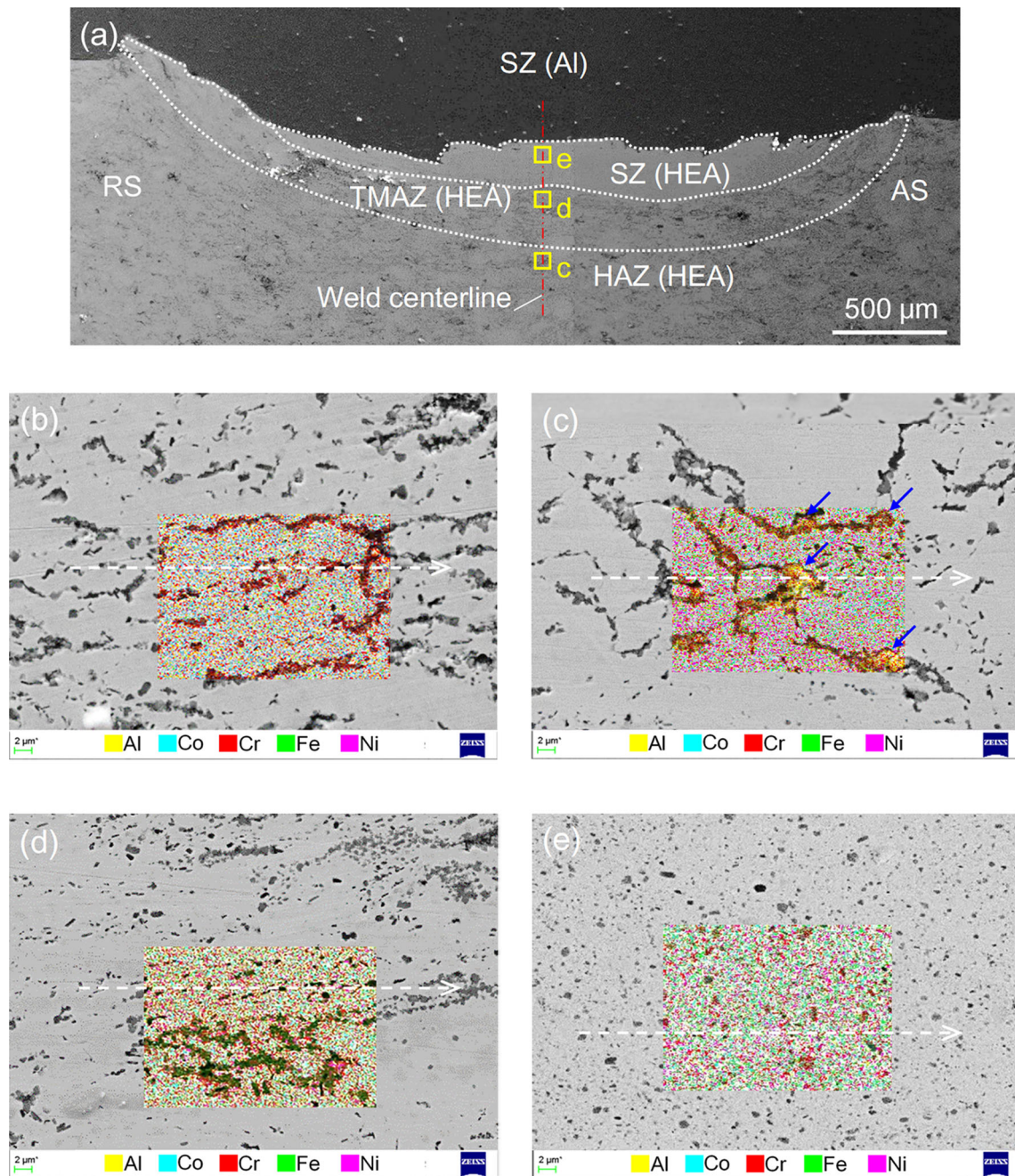


Fig. 2 Microstructures of the HEA in different zones: **a** enlarged view of the lap joint, **b** BM, **c–e** HAZ, TMAZ and SZ corresponding to locations (**c–e**) of (**a**), respectively

thermo-mechanically affected zone (TMAZ) and heat affected zone (HAZ) according to the different microstructure features. The spherical pin tip is inserted into the lower HEA upto a depth of 0.25 mm during the welding, leading to a crescent-shaped SZ with a maximum thickness of ~ 0.25 mm. The TMAZ of HEA is also crescent-shaped beneath the SZ. The deformed zones (SZ and TMAZ) at the AS are thicker than those at the RS due

to the more intense tool-workpiece interaction at the AS during FSW.

Figure 2**b–e** shows the microstructures extracted from the BM and the locations **c–e** marked in Fig. 2**a**, respectively. Two typical powder metallurgy structures are distinct in the BM. One is the bulk structure with light color and the other is the accumulated network structure with dark color. EDS analysis reveals that the light bulk structure is rich in four elements: Co, Cr, Fe and Ni, but has a

small amount of Al (Al-0.7, Co-25.1, Cr-25.2, Fe-25.3, Ni-23.7, all in at%), while the dark network structure is rich in Al and Cr (Al-18.3, Co-7.6, Cr-59.4, Fe-8.2, Ni-6.3, all in at%). The element mapping highlighted in the BM clearly shows that Al and Cr co-segregate to the network structures (see Figs. 2b, 3a, d). Co, Fe and Ni are depleted in the same regions but distributed in the light bulk structures in a relatively homogeneous pattern. Such element distribution feature is further verified by the line scan along the white dash arrow shown in Fig. 2b, where the concentration of Cr is the most significant one in the network structures followed by Al (see Fig. 4a).

The mechanical alloying is a nonequilibrium process where the element segregation is commonly caused by the short sintering duration during the preparation of HEA [16, 19, 20]. The complex compositions and sluggish diffusion of multiple principal elements also contribute to the inhomogeneity of HEAs. From the viewpoint of equilibrium thermodynamics, element segregation comes about to minimize the mixing Gibb's free energy of a solid-solution HEA. The imperfections in the HEA are thermodynamically susceptible to attract atoms to reduce the system's free energy. Sun et al.'s study on $Al_{1.5}CrFeNi$ confirming the effects of atom size on diffusion is applicable to HEAs [21]. The activation energy for migration of Cr is found to be the lowest followed by that of Co, Fe and Ni in the investigation on CrCoFeNi HEA of Middleburgh et al. [22]. Actually, the oversized atoms can move faster than the undersized atoms under the vacancy-solute exchange mechanism in alloys due to the effect of bonding characteristics of the electrons [23]. Consequently, the large-sized

elements Al and Cr tend to segregate to form the dark network structures during the preparation of HEA, while the small-sized elements Fe, Ni and Co as the gradually slower diffuser are mainly distributed in the bulk structures.

In the HAZ, the Al and Cr elements show segregations of higher degrees under further thermodynamic driving force (see Figs. 2c, 3b, e, 4b), leading to the formation of larger-sized Al(Cr)-rich particles, as indicated by blue arrows in Fig. 2c. It can be seen that the accumulated network structures of HAZ present lower distribution densities than those of BM. This means that the enlargement of the Al(Cr)-rich particles is actually dependent on the dissolution of the small-sized particles and the element diffusion from the solid-solution atoms.

Compared with the non-deformed zones of the joint (BM and HAZ), the network structures are dispersed into small-sized particles in the TMAZ, and the particles are accumulated and distributed along a certain direction, i.e., the extrusion direction of the deformed material of the TMAZ (see Fig. 2d). The element distributions in TMAZ exhibit relatively homogeneous feature in contrast to those in BM and HAZ due to the effect of material plastic deformation (see Figs. 3c, f, 4c). As for SZ, finer and more uniformly distributed microstructures have been produced under the direct tool stirring action, and thus, the content fluctuation of each element has been reduced to a rather low level (see Figs. 2e, 4d).

For HEAs, the structure type is the dominant factor that controls the mechanical property of the alloy. The hardness test is conducted on the cross section and the hardness

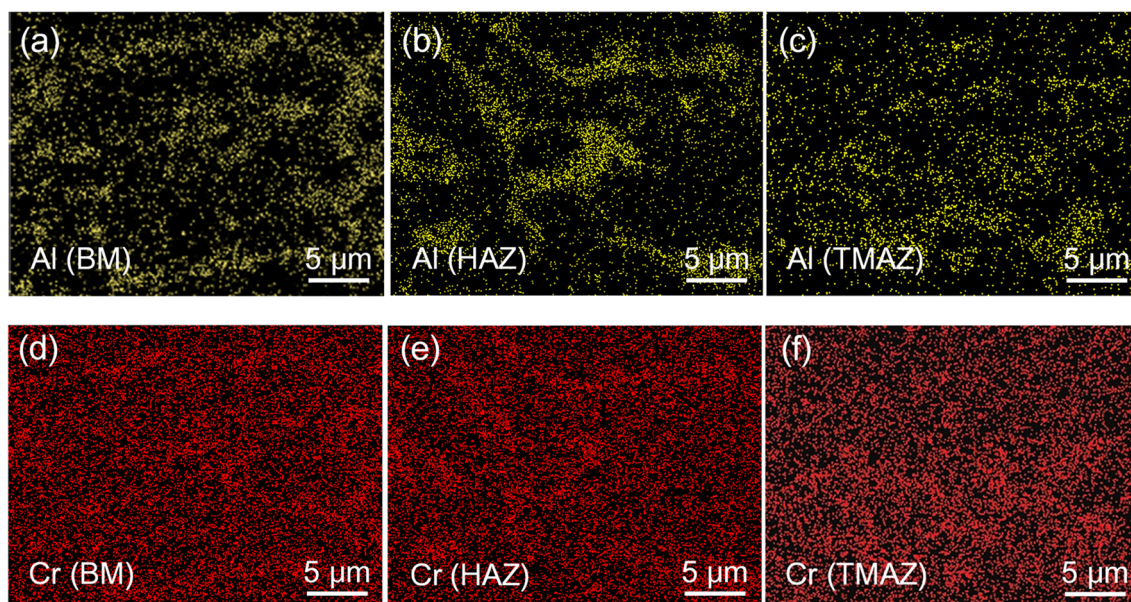
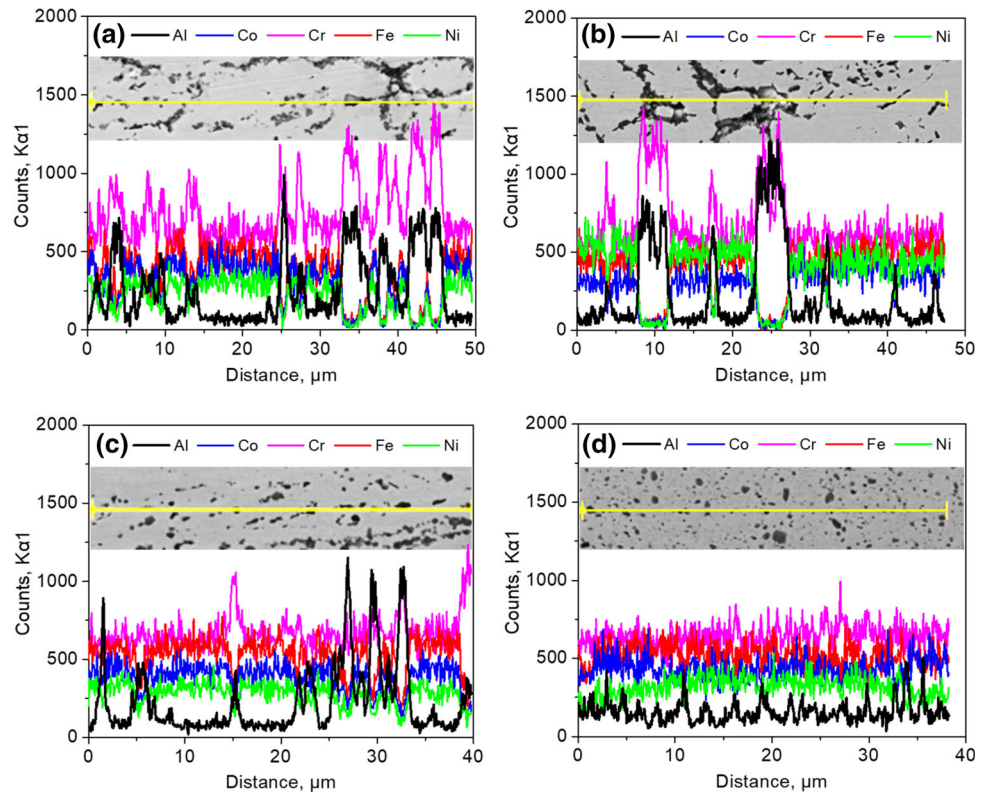


Fig. 3 EDS mappings for Al and Cr of the HEA in different zones: **a–c** Al in the BM, HAZ and TMAZ, respectively, **d–f** Cr in the BM, HAZ and TMAZ, respectively

Fig. 4 Line scans for different zones made along the white dash arrows indicated in Fig. 2: **a** BM, **b** HAZ, **c** TMAZ and **d** SZ



contour map is plotted in Fig. 5. As far as the pure aluminum is concerned, the grain size is the main factor that governs the weld hardness, and thus, the deformed zones (TMAZ + SZ) composed of refined grains show hardness improvements in contrast to the Al BM. In comparison, the hardness evolution in the HEA weld and the underlying reasons are more complicated and more focus has been paid on these factors in this study. It can be seen that the TMAZ and HAZ of HEA are harder than the HEA BM. The enhanced solid-solution strengthening due to dissolution of small-size network structures should be responsible for the hardness improvement in the HAZ. The structure refinement and improvement in strain hardening effect

induced by the plastic deformation should contribute to higher hardness improvement in the TMAZ.

The SZ of HEA exhibits evidently higher hardness than the other zones, which possesses an average hardness over 400 Hv. The maximum hardness of SZ has reached 600 Hv, which is located at the AS where severe plastic deformation occurs during FSLW. As mentioned above, the positive effects of grain refinement by FSW on the strength improvement in $Al_xCoCrFeNi$ alloys have been verified by previous studies. A $CoCrFeNiAl_{0.3}$ alloy was friction stir welded by Zhu et al., and it was demonstrated that the SZ showed higher hardness (220 Hv) than the BM (180 Hv) due to the grain refinement [12]. Kumar et al. also found that the hardness of SZ increases from 132 to 244 Hv after the friction stir processing of $Al_{0.1}CoCrFeNi$ alloy [24]. On the contrary, the SZ of $Al_{0.1}CoCrFeNi$ HEA here exhibits an average hardness improvement of ~ 300 Hv in contrast to the BM with hardness of ~ 100 Hv, which reflects that the operative strengthening mechanisms are more complicated than pure grain refinement.

A large number of studies have shown that the hardness of $Al_xCoCrFeNi$ HEA is largely related to the Al content [25–27]. It has been verified that the maximum hardness of the alloy can reach nearly 550 Hv by varying the value of x [27]. Obviously, much higher hardness of 600 Hv has been achieved in this study. In addition to the structure refinement, the Al content and the induced structure

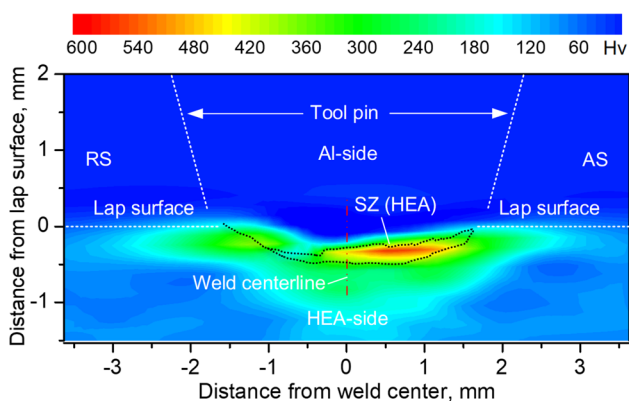


Fig. 5 Hardness contour map of the lap joint

evolution should also be considered and illustrated. In order to further illuminate the rather high hardness in the SZ of HEA, Fig. 6 presents the element mapping at the Al-HEA interface on weld centerline. It can be seen that Co, Cr, Fe and Ni are rarely distributed in the Al-side, while obvious Al element can be observed in the HEA-side. The line scan of Al element reveals that the Al content shows little variation from HAZ to TMAZ but increases significantly after the curve enters SZ in the HEA (see Fig. 7). That is to say, the FSLW of Al and HEA has improved the Al content in the HEA. The diffusion of Al from the upper Al sheet toward the lower HEA sheet should be limited due to the slow-diffusion effect of HEA [28], nevertheless, the downward flow of aluminum and its mixing with the HEA during FSW will contribute to the improvement in Al content in the SZ.

The Al content has remarkable effect on the crystal lattice structure of HEA. The lap joint was fractured through the lap interface during tensile shear test, and thus, XRD analyses were performed on the fracture surface at SZ of the failed joint to determine the crystal lattice structures of the SZ. The results are given in Fig. 8. The HEA BM is defined as FCC phase. In comparison, the intensity of diffraction peak exhibits a weakening in FCC phase but meanwhile an enhancement in BCC phase in the SZ. Previous research on $\text{Al}_x\text{CoCrFeNi}$ alloy pointed out that the phase structure of HEA did not change by only FSW [12]. Therefore, the BCC phase should be transformed from the FCC phase of HEA BM due to the increase in Al content. For HEAs, each element has the same possibility to occupy the lattice site, and the lattice distortion comes from the different atom sizes that make up

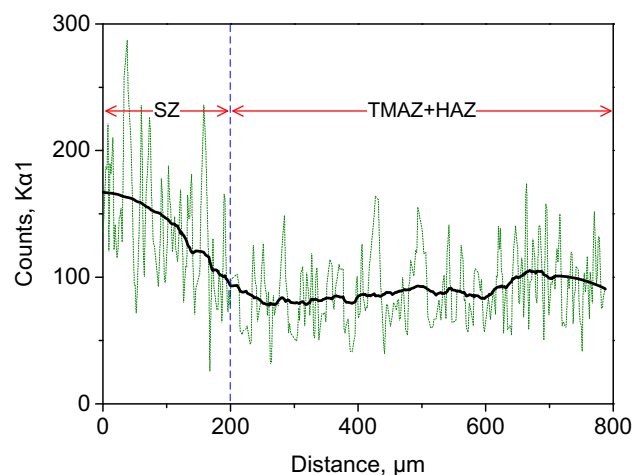
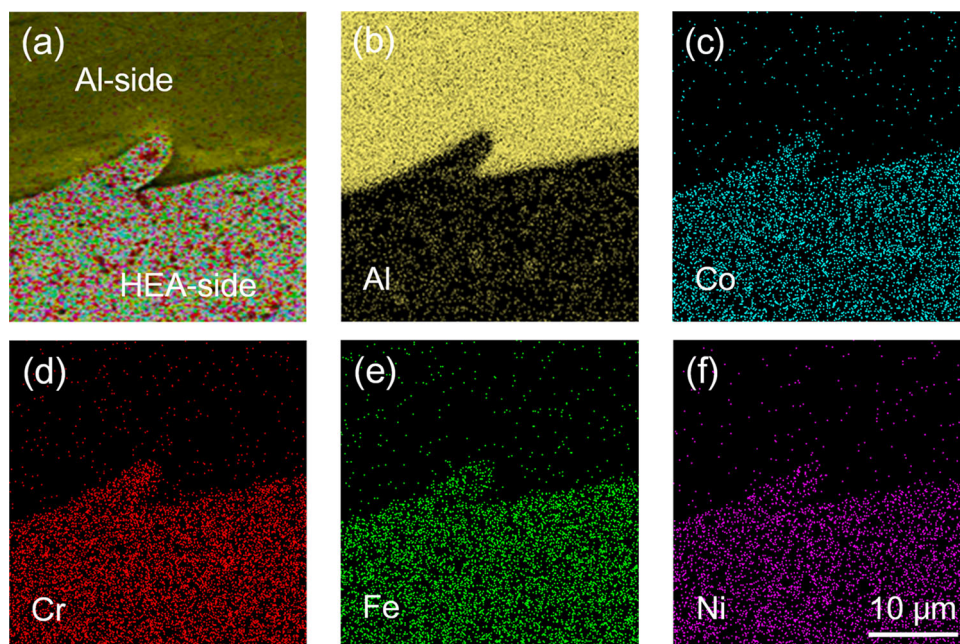


Fig. 7 Line scan of Al in HEA made along weld centerline

the crystal lattices. Due to the large atomic radius of Al, the increase in Al content should lead to an increase in lattice constant and thus larger lattice strains. Since BCC is not a close-packed structure, the structural transformation from the initial FCC to BCC then occurs at higher Al content in order to reduce the lattice distortion induced by the atomic size mismatch of constituent elements.

In addition to the fine grain strengthening that has been widely ascertained, aluminum addition during the FSLW provides other strategies for the hardness improvement in the HEA. On one hand, additional solid-solution strengthening effect is introduced to the SZ owing to the content improvement in Al element. On the other hand, the increase in Al content induces the occurrence of BCC phase. The BCC cell with lower packing factor is able to

Fig. 6 EDS mappings for various elements at Al-HEA interface on weld centerline: **a** element composition diagram, **b** Al, **c** Co, **d** Cr, **e** Fe and **f** Ni



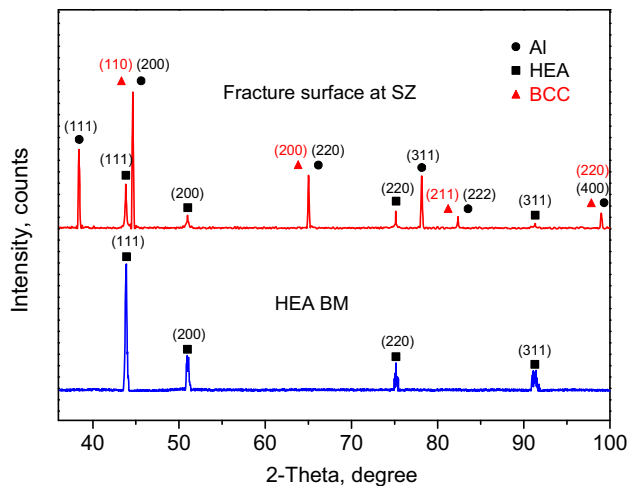


Fig. 8 XRD analysis results of HEA BM and the fracture surface at SZ

ease the lattice distortion caused by the large atomic radius of Al, resulting in the strong lattice distortion and the high hardness of the alloy [29–31]. Consequently, the SZ having much higher hardness is produced in the HEA.

The traditional problems such as coarsening of microstructures, inhomogeneity of element distributions and poor mechanical properties are always the main concerns for the preparation of HEAs. Thermo-mechanical processing of HEAs including cold rolling and annealing has been investigated by several researchers recently in order to solve these problems, where the alloys are firstly cold rolled to improve the stored dislocation energy and then annealed for partially or completely recrystallization [32–34]. In comparison, FSW appears to be a more effective approach for the improvement in microstructures and mechanical properties of HEAs as the thermal and mechanical effects from welding tool are simultaneously exerted to the alloys during the welding. However, the existing studies have shown that only FSW has the limited effect on the hardness improvement in $Al_xCoCrFeNi$ HEAs. Both advantages of friction stir modification and Al content improvement are integrated by the FSLW of Al and HEA in the present research, leading to superior hardness values in the $Al_{0.1}CoCrFeNi$. The present study is expected to be able to provide an applicable method for the preparation and strengthening of HEAs via adjusting the chemical compositions through FSW.

4 Conclusions

Based on the investigations above mentioned, the conclusions of significance are drawn as follows:

- (1) Crescent-shaped deformed zones are formed in the HEA during the FSLW of Al and HEA. The hook and cold lap defects commonly present in friction stir lap welds are not observed at the Al-HEA interface due to the limited flow of HEA material.
- (2) The HEA BM is characterized by co-segregation of Al and Cr to network structures. Coarsening of large-sized Al(Cr)-rich particles and dissolution of small-sized Al(Cr)-rich particles take place in the HAZ of HEA. The enhancement of solid-solution strengthening leads to higher hardness of HAZ relative to the BM.
- (3) The plastic deformation during FSW refines and homogenizes the microstructures in the TMAZ and SZ of HEA, which contributes to higher hardness in both the zones. The hardness of SZ is improved to a maximum of 600 Hv, higher than that of $Al_xCoCrFeNi$ traditionally obtained at various x values.
- (4) Al content is improved in the SZ of HEA during the Al-HEA FSLW, leading to the enhancement of solid-solution strengthening and the occurrence of BCC structures in the SZ. Associated with microstructure refinement, the comprehensive strengthening effects are responsible for the superior hardness of the SZ.

Acknowledgements The authors are grateful to be supported by Natural Science Foundation of Hebei Province (No. E2020501021), Fundamental Research Funds for the Central Universities (No. N2023028) and Program for the Top Young Talents of Higher Learning Institutions of Hebei Province (No. BJ2019201).

References

1. Tsai M H, *Entropy* **15** (2013) 5338.
2. Zhang Y, Zuo T T, Tang Z, Gao M C, Dahmen K A, Liaw P K, and Lu Z P, *Prog Mater Sci* **61** (2014) 1.
3. Saikumar A, Mythili R, Saroja S, and Srihari V, *T Indian I Metals* **72** (2019) 111.
4. Zharebtsov S, Stepanov N, Shaysultanov D, Malopheyev S, Vysotskiy I, Sanin V, Kashaev N, and Kaibyshev R, *Mater Sci Forum* **941** (2018) 919.
5. Sokkalingam R, Mishra S, Cheethirala S R, Muthupandi V, and Sivaprasad K, *Metall Mater Trans A* **48** (2017) 3630.
6. Wu Z, David S A, Leonard D N, Feng Z, and Bei H, *Sci Technol Weld Join* **23** (2018) 585.
7. Kashaev N, Ventzke V, Stepanov N, Shaysultanov D, Sanin V, and Zharebtsov S, *Intermetallics* **96** (2018) 63.
8. Nam H, Park C, Moon J, Na Y, Kim H, and Kang N, *Mater Sci Eng A* **742** (2019) 224.
9. Wu Z, David S A, Feng Z, and Bei H, *Scr Mater* **124** (2016) 81.
10. Zharebtsov D, Stepanov N, Malopheyev S, Vysotskiy I, Sanin V, Mironov S, Kaibyshev R, Salishchev G, and Zharebtsov S, *Mater Charact* **145** (2018) 353.
11. Jo M G, Kim H J, Kang M, Madakashira P P, Park E S, Suh J Y, Kim D I, Hong S T, and Han H N, *Met Mater Int* **24** (2018) 73.
12. Zhu Z G, Sun Y F, Goh M H, Ng F L, Nguyen Q B, Fujii H, Nai S M L, Wei J, and Shek C H, *Mater Lett* **205** (2017) 142.

13. Zhu Z G, Sun Y F, Ng F L, Goh M H, Liaw P K, Fujii H, Nguyen Q B, Xu Y, Shek C H, Nai S M L, and Wei J, *Mater Sci Eng A* **711** (2018) 524.
14. Meng X, Huang Y, Cao J, Shen J, and dos Santos J F, *Prog Mater Sci* **115** (2021) 100706.
15. Liu B, Wang J, Liu Y, Fang Q, Wu Y, Chen S, and Liu C T, *Intermetallics* **75** (2016) 25.
16. Zhang K B, Fu Z Y, Zhang J Y, Wang W M, Lee S W, and Niihara K, *J Alloy Compd* **495** (2010) 33.
17. Huang Y X, Wang J C, Wan L, Meng X C, Liu H B, and Li H, *Mater Lett* **185** (2016) 181.
18. Huang Y X, Huang T F, Wan L, Meng X C, and Zhou L, *J Mater Process Tech* **263** (2019) 129.
19. Praveen S, Murty B S, and Kottada R S, *Mater Sci Eng A* **534** (2012) 83.
20. Yu H Y, Fang W, Chang R B, Ji P G, and Wang Q Z, *T Nonferr Metal Soc* **29** (2019) 2331.
21. Sun S, Qiu N, Zhang K, He P N, Ma Y J, Gou F J, and Wang Y, *Scr Mater* **161** (2019) 40.
22. Middleburgh S C, King D M, Lumpkin G R, Cortie M, and Edwards L, *J Alloy Compd* **599** (2014) 179.
23. Janotti A, Kremer M, Fu C L, and Reed R C, *Phys Rev Lett* **92** (2004) 085901.
24. Kumar N, Komarasamy M, Nelaturu P, Tang Z, Liaw P K, and Mishra R S, *JOM* **67** (2015) 1007.
25. Yang T, Xia S, Liu S, Wang C, Liu S, Zhang Y, Xue J, Yan S, and Wang Y, *Mater Sci Eng A* **648** (2015) 15.
26. Wang W R, Wang W L, Wang S C, Tsai Y C, Lai C H, and Yeh J W, *Intermetallics* **26** (2012) 44.
27. Kao Y F, Chen T J, Chen S K, and Yeh J W, *J Alloy Compd* **488** (2009) 57.
28. Zhang Y, Lu Z P, Ma S G, Liaw P K, Tang Z, Cheng Y Q, and Gao M C, *MRS Commun* **4** (2014) 57.
29. Li B Y, Peng K, Hu A P, Zhou L P, Zhu J J, and Li D Y, *T Nonferr Metal Soc* **23** (2013) 735.
30. Toda-Caraballo I, and Rivera-Díaz-del-Castillo P E J, *Intermetallics* **71** (2016) 76.
31. Yeh J W, Chen S K, Lin S J, Gan J Y, Chin T S, Shun T T, Tsau C H, and Chang S Y, *Adv Eng Mater* **6** (2004) 299.
32. Hou J X, Shi X H, Qiao J W, Zhang Y, Liaw P K, and Wu Y C, *Mater Des* **180** (2019) 107910.
33. Li Z Y, Fu L M, Peng J, Zheng H, and Shan A D, *Mater Sci Eng A* **786** (2020) 139446.
34. Xie Y H, Liang J M, Zhang D L, Luo Y F, Zhang Z, Liu Y, and Wang J, *Scripta Mater* **187** (2020) 390.

Publisher's Note Springer Nature remains neutral with regard to jurisdictional claims in published maps and institutional affiliations.